Acta Mechanica Sinica (2014) 30(4):507–515
DOI 10.1007/s10409-014-0067-0

RESEARCH PAPER

Analysis of bending and buckling of pre-twisted beams: A bioinspired study

Zi-Long Zhao · Hong-Ping Zhao · Zheng Chang · Xi-Qiao Feng

Received: 28 March 2014 / Revised: 4 May 2014 / Accepted: 10 June 2014

Abstract Twisting chirality is widely observed in artificial and natural materials and structures at different length scales. In this paper, we theoretically investigate the effect of twisting chiral morphology on the mechanical properties of elastic beams by using the Timoshenko beam model. Particular attention is paid to the transverse bending and axial buckling of a pre-twisted rectangular beam. The analytical solution is first derived for the deflection of a clamped-free beam under a uniformly or periodically distributed transverse force. The critical buckling condition of the beam subjected to its self-weight and an axial compressive force is further solved. The results show that the twisting morphology can significantly improve the resistance of beams to both transverse bending and axial buckling. This study helps understand some phenomena associated with twisting chirality in nature and provides inspirations for the design of novel devices and structures.

Keywords Twisting chirality · Timoshenko beam · Bending · Euler buckling · Bionics

The project was supported by the National Natural Science Foundation of China (31270989 and 11372162), the 973 Program of MOST (2010CB631005 and 2012CB934001), and Tsinghua University (20121087991).

Z.-L. Zhao · H.-P. Zhao · Z. Chang · X.-Q. Feng (✉)
Institute of Biomechanics and Medical Engineering,
AML, Department of Engineering Mechanics,
Tsinghua University, 100084 Beijing, China
e-mail: fengxq@tsinghua.edu.cn

Z.-L. Zhao · X.-Q. Feng
Center for Nano and Micro Mechanics,
Tsinghua University, 100084 Beijing, China

1 Introduction

Twisting chirality is ubiquitous in both artificial and biological materials and structures at different length scales. For examples, gemini surfactants [1], chiral polymers [2], and nanocrystalline materials [3] can self-assemble into twisted ribbons. Most biological macromolecules (e.g., DNA, RNA, and proteins) also take helical morphologies [4, 5]. Some biological cells (e.g., spirally striated muscle cells in invertebrates [6]), bacteria (e.g., Helicobacter pylori [7]), and tissues (e.g., Towel Gourd tendrils [8]) have helical shapes, which are of crucial significance to achieve their biological functions [9, 10]. For illustration, Fig. 1a shows some twisting carbon nanostructures prepared on a glass substrate using sputter-coated Fe-base alloy catalysts [11], and Fig. 1b shows a *Paphiopedilum dianthum* flower with twisting petals [12], respectively. Besides, twisting structures have technologically important applications in the fields of aviation and engineering, e.g., helicopter blades, turbine blades, propellers, and gears.

In theoretical analysis, twisting structures are commonly modeled as pre-twisted bars, rods, or beams. Carnegie [13, 14], Lin and Hsiao [15], and Zhu [16] analyzed the vibration of pre-twisted blades for satellite booms and aircraft rotary wings by employing both Euler's and Timoshenko's beam models. Schulgasser and Witztum [9] focused on the stability of slender leaves with chiral configurations, e.g., *Pancratium*. Recently, Ye et al. [2] and Wang et al. [17] investigated, both experimentally and theoretically the surface stress effect on the twisting chirality of lamellar crystals and nanomaterials by using a refined Kirchhoff rod model.

The transverse bending and axial buckling behaviors of twisted materials are an issue of particular interest. Carnegie [18] theoretically and experimentally examined the

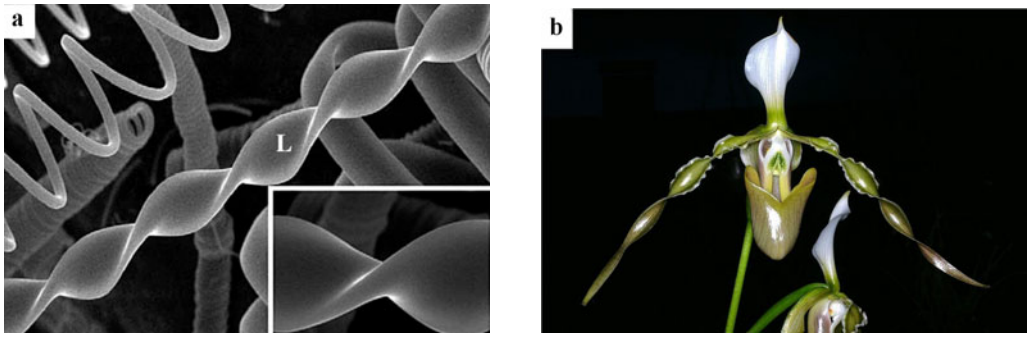

Fig. 1 **a** A twisting micro-ribbon produced by Ni catalyst under a magnetic field [11]; **b** Twisting flower petals of *Paphiopedilum dianthum* [12]

static bending of pre-twisted cantilever beams with different twist angles from 0° to 90°. Subrahmanyam et al. [19] accounted for the effect of transverse shear deformation and Abid et al. [20] performed finite element simulations to investigate the bending properties of pre-twisted beams. Recently, Chen [21, 22] analyzed the bending deflections of a pre-twisted beam subjected to uniformly distributed transverse forces. Ziegler [23, 24] derived the Euler buckling equations of a pre-twisted beam, and Lüscher [25] solved them for the case of cantilever beam. Leipholz [26] and Nixdorff [27] analyzed the axial buckling of a pre-twisted elastic rod based on the Kirchhoff rod theory. Considering the effect of shear deformation, Tabarrok et al. [28] provided the governing equations for the buckling of a pre-twisted beam under axial compression. Despite of these previous simplified studies, it remains elusive how the twisting chirality of a beam affects its mechanical properties and why many plants (e.g., *Typha* and *Narcissus*) take the twisting morphologies.

In practical environments, aquatic macrophytes are subjected to both self-weight and wind loads. Through millions of years of evolution by natural selection, the emergent bulks of some aquatic macrophytes have formed an optimal morphology with enhanced mechanical properties. In the present paper, inspired by these natural phenomena, we analyze the transverse bending and axial buckling of a pre-twisted beam by using the Timoshenko beam model. The deflection of a clamped-free beam under a uniformly or periodically distributed transverse force is first derived in an explicit form. The critical buckling condition of the beam subjected to both self-weight and axial compression is subsequently solved. The effects of twist angle, cross-sectional aspect ratio, and loading conditions are examined. The results demonstrate that twisting a rectangular beam into a chiral morphology can improve its resistance ability to both transverse bending and axial buckling.

2 Theoretical model

A pre-twisted rectangular beam is sketched in Fig. 2a. Let b, h, and L denote respectively its width, thickness, and length, with $b \geqslant h$. The beam has a twist angle $\theta = \overline{\theta}L$, where $\overline{\theta}$ denotes the twist angle per unit length along the longitudinal direction. Denote the cross-sectional aspect ratio of the beam as

$$\mu = \frac{b}{h}. \tag{1}$$

Refer to a Cartesian coordinate system (x, y, z), as shown in Fig. 2b, where $\{\boldsymbol{i}, \boldsymbol{j}, \boldsymbol{k}\}$ are the orthonormal unit basis vectors, the origin o is located at the cross-sectional centroid at the clamped end of the beam, x, y, and z axes are parallel to the width, thickness, and length directions, respectively. Besides, we introduce a twist coordinate system (X, Y, Z) fixed to the cross section of the beam. The Z axis coincides with z, while the rotating X and Y axes are along the two cross-sectional principal directions of the beam.

In terminology of the Timoshenko beam theory, introduce four generalized displacements: u_x and u_y denote the deflections of the cross-sectional centroid, ϕ_x and ϕ_y denote the rotating angles of its cross section in the x and y directions, respectively. As shown in Fig. 2c, the cross section has the pre-existed rotating angle $\overline{\theta}z$ about the z axis. The normal strain at position (x, y, z) is written as

$$\varepsilon_z = x\frac{\mathrm{d}\phi_y}{\mathrm{d}z} + y\frac{\mathrm{d}\phi_x}{\mathrm{d}z}. \tag{2}$$

Assume that the material is linear elastic and isotropic. Then the bending moments M_x and M_y along the x and y directions on the cross section can be derived as

$$\begin{aligned} M_x &= \iint_A E\varepsilon_z y \mathrm{d}A = EI_{xx}\frac{\mathrm{d}\phi_x}{\mathrm{d}z} + EI_{xy}\frac{\mathrm{d}\phi_y}{\mathrm{d}z}, \\ M_y &= \iint_A E\varepsilon_z x \mathrm{d}A = EI_{xy}\frac{\mathrm{d}\phi_x}{\mathrm{d}z} + EI_{yy}\frac{\mathrm{d}\phi_y}{\mathrm{d}z}, \end{aligned} \tag{3}$$

where E is the Young's modulus and A represents the cross-sectional area of the beam. The area moments of inertia I_{xx} and I_{yy}, and the polar moment of area I_{xy} are expressed as

$$\begin{aligned} I_{xx} &= I_X \cos^2(\overline{\theta}z) + I_Y \sin^2(\overline{\theta}z), \\ I_{yy} &= I_X \sin^2(\overline{\theta}z) + I_Y \cos^2(\overline{\theta}z), \\ I_{xy} &= (I_Y - I_X)\sin(\overline{\theta}z)\cos(\overline{\theta}z), \end{aligned} \tag{4}$$

respectively, where $I_X = bh^3/12$ and $I_Y = b^3h/12$ designate the principal area moments of inertia of the cross section.

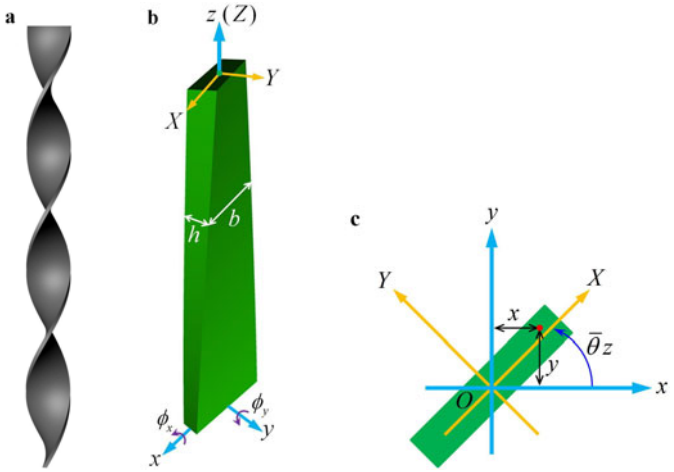

Fig. 2 **a** A pre-twisted rectangular cantilever beam; **b** Its model with the global coordinate system (x, y, z) and local coordinate system (X, Y, Z), and **c** the rectangular cross section

We analyze the pre-twisted beam by using the principle of minimum potential energy. The elastic strain energy of the beam due to bending can be calculated by

$$U_{\mathrm{b}} = \frac{1}{2}\int_0^L \left[EI_{xx}\left(\frac{\mathrm{d}\phi_x}{\mathrm{d}z}\right)^2 + 2EI_{xy}\frac{\mathrm{d}\phi_x}{\mathrm{d}z}\frac{\mathrm{d}\phi_y}{\mathrm{d}z} + EI_{yy}\left(\frac{\mathrm{d}\phi_y}{\mathrm{d}z}\right)^2\right]\mathrm{d}z. \tag{5}$$

Besides, the elastic strain energy U_{s} of the beam due to shear deformation is

$$U_{\mathrm{s}} = \frac{1}{2}\int_0^L \kappa GA\left[\left(\frac{\mathrm{d}u_x}{\mathrm{d}z} - \phi_y\right)^2 + \left(\frac{\mathrm{d}u_y}{\mathrm{d}z} - \phi_x\right)^2\right]\mathrm{d}z, \tag{6}$$

where $G = E/[2(1+\nu)]$ is the shear modulus and κ is the shearing correction factor. For rectangular beams, κ is ascertained as 0.83 [29]. Consequently, the total elastic strain energy U of the beam is

$$U = U_{\mathrm{b}} + U_{\mathrm{s}}. \tag{7}$$

3 Bending

Many twisting materials are subjected to distributed transverse loads along the length direction, e.g., the leaves of plants and flower petals in wind, the rotary wings in airflow, and the propellers in stream. Transverse loads applied on the pre-twisted beams are often in a periodical form along the longitudinal direction. Therefore, we here investigate the bending property of the pre-twisted cantilever beam subjected to periodically distributed transverse force. The uniformly distributed force is one of its degenerated cases. Suppose that the transverse force passes through the neutral axis, i.e., z. We first derive the analytical solution for the case of the transverse force $\boldsymbol{f}$ in the y direction, i.e.,

$$\boldsymbol{f}(z) = f_y(z)\boldsymbol{j}. \tag{8}$$

For illustration, assume that the force acting on the beam is proportional to the upstream area. Then the transverse force f_y with intensity $\overline{f}_y$ per unit area has the form of

$$f_y = f_1 + f_2|\cos(\overline{\theta}z)|, \quad 0 \leqslant z \leqslant L, \tag{9}$$

where $f_1 = h\overline{f}_y$ and $f_2 = (b-h)\overline{f}_y$. The form of forces in Eq. (9) can be easily extended to more general distributed forces by using the Fourier series expansion, as will be shown below. When $0^\circ \leqslant \theta \leqslant 90^\circ$, the potential energy V_f of the external forces is written as

$$V_f = -\int_0^L [f_1 + f_2\cos(\overline{\theta}z)]u_y\mathrm{d}z. \tag{10}$$

Let $\Pi = U + V_f$ denote the total potential energy of the beam system. According to the principle of minimum potential energy, the beam at the equilibrium state has the following variational relation

$$\delta\Pi = \delta(U + V_f) = 0. \tag{11}$$

Note that due to the chiral morphology of the beam, the force in the y direction will induce both deflections in the x and y directions, u_x and u_y. Substituting Eqs. (7) and (10) into Eq. (11) leads to a set of static equilibrium equations of the pre-twisted cantilever beam

$$\begin{aligned}
&\frac{\mathrm{d}^2u_x}{\mathrm{d}z^2} = \frac{\mathrm{d}\phi_y}{\mathrm{d}z},\\
&\frac{\mathrm{d}^2u_y}{\mathrm{d}z^2} = -\frac{f_1 + f_2\cos(\overline{\theta}z)}{\kappa GA} + \frac{\mathrm{d}\phi_x}{\mathrm{d}z},\\
&\frac{\mathrm{d}}{\mathrm{d}z}\left(I_{xx}\frac{\mathrm{d}\phi_x}{\mathrm{d}z} + I_{xy}\frac{\mathrm{d}\phi_y}{\mathrm{d}z}\right) = \frac{\kappa GA}{E}\left(\phi_x - \frac{\mathrm{d}u_y}{\mathrm{d}z}\right),\\
&\frac{\mathrm{d}}{\mathrm{d}z}\left(I_{xy}\frac{\mathrm{d}\phi_x}{\mathrm{d}z} + I_{yy}\frac{\mathrm{d}\phi_y}{\mathrm{d}z}\right) = \frac{\kappa GA}{E}\left(\phi_y - \frac{\mathrm{d}u_x}{\mathrm{d}z}\right),
\end{aligned} \tag{12}$$

and eight boundary conditions at $z = 0$ and $z = L$

$$u_x|_{z=0} = u_y\big|_{z=0} = \phi_x|_{z=0} = \phi_y\big|_{z=0} = 0, \tag{13}$$

$$\kappa GA\left(\frac{\mathrm{d}u_x}{\mathrm{d}z}-\phi_y\right)\Big|_{z=L} = \kappa GA\left(\frac{\mathrm{d}u_y}{\mathrm{d}z}-\phi_x\right)\Big|_{z=L}$$
$$= \left(EI_{xx}\frac{\mathrm{d}\phi_x}{\mathrm{d}z}+EI_{xy}\frac{\mathrm{d}\phi_y}{\mathrm{d}z}\right)\Big|_{z=L}$$
$$= \left(EI_{yy}\frac{\mathrm{d}\phi_y}{\mathrm{d}z}+EI_{xy}\frac{\mathrm{d}\phi_x}{\mathrm{d}z}\right)\Big|_{z=L}=0. \quad (14)$$

Now we attempt to solve the deflections u_x and u_y in terms of the coupled ordinary differential equations. Using the free-end ($z = L$) boundary conditions in Eq. (14), the static equilibrium equations (12) are recast as

$$\begin{aligned}
&\frac{\mathrm{d}u_x}{\mathrm{d}z}=\phi_y,\\
&\frac{\mathrm{d}u_y}{\mathrm{d}z}=\frac{f_1\overline{\theta}(L-z)+f_2[\sin(\overline{\theta}L)-\sin(\overline{\theta}z)]}{\kappa GA\overline{\theta}}+\phi_x,\\
&I_{xx}\frac{\mathrm{d}\phi_x}{\mathrm{d}z}+I_{xy}\frac{\mathrm{d}\phi_y}{\mathrm{d}z}=\frac{f_1(L-z)^2}{2E}\\
&\qquad+\frac{f_2[\cos(\overline{\theta}L)-\cos(\overline{\theta}z)+\overline{\theta}\sin(\overline{\theta}L)(L-z)]}{E\overline{\theta}^2},\\
&I_{xy}\frac{\mathrm{d}\phi_x}{\mathrm{d}z}+I_{yy}\frac{\mathrm{d}\phi_y}{\mathrm{d}z}=0.
\end{aligned} \quad (15)$$

The area moments of inertia I_{xx} and I_{yy} and the polar moment of area I_{xy} in Eq. (15) can be expressed by the principal moments of inertia I_X and I_Y from Eq. (4). Substituting the clamped-end ($z = 0$) boundary conditions into Eq. (15) leads to the following relations

$$\begin{aligned}
&\frac{\mathrm{d}^2u_x}{\mathrm{d}z^2}=\frac{(I_X-I_Y)\sin(2\overline{\theta}z)}{4I_XI_YE}f_1(L-z)^2\\
&\qquad+\frac{(I_X-I_Y)\sin(2\overline{\theta}z)}{2I_XI_YE\overline{\theta}^2}\\
&\qquad\times f_2[\cos(\overline{\theta}L)-\cos(\overline{\theta}z)+\overline{\theta}\sin(\overline{\theta}L)(L-z)],\\
&u_x|_{z=0}=0,\quad \frac{\mathrm{d}u_x}{\mathrm{d}z}\Big|_{z=0}=0,\\
&\frac{\mathrm{d}^2u_y}{\mathrm{d}z^2}=-\frac{f_1+f_2\cos(\overline{\theta}z)}{\kappa GA}\\
&\qquad+\frac{I_X\sin^2(\overline{\theta}z)+I_Y\cos^2(\overline{\theta}z)}{2I_XI_YE}f_1(L-z)^2\\
&\qquad+\frac{I_X\sin^2(\overline{\theta}z)+I_Y\cos^2(\overline{\theta}z)}{I_XI_YE\overline{\theta}^2}\\
&\qquad\times f_2[\cos(\overline{\theta}L)-\cos(\overline{\theta}z)+\overline{\theta}\sin(\overline{\theta}L)(L-z)],\\
&u_y\big|_{z=0}=0,\quad \frac{\mathrm{d}u_y}{\mathrm{d}z}\Big|_{z=0}=\frac{f_1\overline{\theta}L+f_2\sin(\overline{\theta}L)}{\kappa GA\overline{\theta}}.
\end{aligned} \quad (16)$$

Thus the governing equations have been translated into two coupled second-order ordinary differential equations with four boundary conditions. From Eq. (16), the deflections in the x and y directions are derived as

$$\begin{aligned}
u_x&=\frac{I_X-I_Y}{144\overline{\theta}^4EI_XI_Y}(9f_1C_{1x}+2f_2C_{2x}),\\
u_y&=\frac{1}{288\overline{\theta}^4EI_Y}(3f_1C_{1y}+f_2C_{2y}),
\end{aligned} \quad (17)$$

where

$$\alpha=\overline{\theta}z,\quad \beta=\frac{EI_Y}{\kappa GAL^2}, \quad (18)$$

and the expressions of C_{1x}, C_{2x}, C_{1y}, and C_{2y} are given in Appendix A.

Thusfar, we have obtained the analytical solution for the deflections of a pre-twisted beam subjected to a periodically distributed transverse force f_y. The force is decomposed into two parts, namely, a constant f_1 and a cosine function $f_2\cos(\overline{\theta}z)$. By letting $f_2 = 0$, the solution in Eq. (17) reduces to the case of uniformly distributed transverse force f_1 [21]. By contrast, if $f_1 = 0$, the solution corresponds to a distributed force f_y expressed by a cosine function. In more general cases, the distributed force exerted on the pre-twisted cantilever beam can be expressed by a series of cosine functions. Then, we can determine the deflections of the beam resorting to the superposition principle. For example, when $\theta > 90°$, the transverse force f_y in Eq. (9) can be expanded as

$$f_y=f_1+f_2\left|\cos(\overline{\theta}z)\right|=f_1+f_2a_0+f_2\sum_{n=1}^{\infty}a_n\cos\left(\frac{n\pi z}{L}\right), \quad (19)$$

where the coefficients a_0 and a_n are given by

$$\begin{aligned}
a_0&=\frac{1}{L}\int_0^L\left|\cos(\overline{\theta}z)\right|\mathrm{d}z=\int_0^1\left|\cos(\theta\overline{z})\right|\mathrm{d}\overline{z},\\
a_n&=\frac{2}{L}\int_0^L\left|\cos(\overline{\theta}z)\right|\cos\left(\frac{n\pi z}{L}\right)\mathrm{d}z\\
&=2\int_0^1\left|\cos(\theta\overline{z})\right|\cos(n\pi\overline{z})\mathrm{d}\overline{z}.
\end{aligned} \quad (20)$$

The normalized coordinate $\overline{z} = z/L$ varies from 0 to 1. Thus it is easy to derive the explicit solution for the displacements u_x and u_y from Eq. (17).

Further we consider the case when the distributed transverse force $\boldsymbol{f}$ is along the x direction. Let θ_0 denote the direction of $\boldsymbol{f}$ measured clockwise from the y direction. When $\theta_0 = 90°$, the force $\boldsymbol{f}$ is expressed as

$$\boldsymbol{f}(z)=f_x(z)\boldsymbol{i}. \quad (21)$$

The transverse force f_x with intensity $\overline{f}_x$ per unit area has the form of

$$f_x=f_3+f_4\left|\cos(\overline{\theta}z)\right|,\quad 0\leqslant z\leqslant L, \quad (22)$$

where $f_3 = b\overline{f}_x$ and $f_4 = (h - b)\overline{f}_x$.

In the case when the pre-twisted beam is only subjected to the distributed transverse force f_x (i.e., $\theta_0 = 90°$). The analytical solutions of the deflections u_x and u_y of the beam can also be readily determined following a similar procedure, which is omitted here for short.

4 Euler buckling

In nature, a slender twisting bulk of such aquatic macrophytes as *Sagittaria trifolia* subjects to not only its own weight but also concentrated forces acting on its upper end (e.g., the weight of head organs). Inspired by this biological phenomenon, we also consider the Euler buckling of a pre-twisted cantilever-free beam subjected to a distributed compressive force (self-weight) $q = \rho g A$ and a concentrated compressive load P acting at the free end, where ρ is the mass density of the beam and g is the gravitational acceleration. By neglecting the axial normal strain ε_z of the beam, the displacement u_z of the cross-sectional centroid in the z direction at $z = \tilde{z}$, caused by the lateral deformations, is calculated by

$$\begin{aligned} u_z(\tilde{z}) &= \int_0^{\tilde{z}} \left[\sqrt{1 - \left(\frac{\mathrm{d}u_x}{\mathrm{d}z}\right)^2 - \left(\frac{\mathrm{d}u_y}{\mathrm{d}z}\right)^2} - 1 \right] \mathrm{d}z \\ &= -\frac{1}{2} \int_0^{\tilde{z}} \left[\left(\frac{\mathrm{d}u_x}{\mathrm{d}z}\right)^2 + \left(\frac{\mathrm{d}u_y}{\mathrm{d}z}\right)^2 \right. \\ &\quad \left. + o\left(\left(\frac{\mathrm{d}u_x}{\mathrm{d}z}\right)^2, \left(\frac{\mathrm{d}u_y}{\mathrm{d}z}\right)^2\right) \right] \mathrm{d}z. \end{aligned} \tag{23}$$

The potential energies of the external forces include

$$\begin{aligned} V_q &= -\frac{qL}{2} \int_0^L \left(1 - \frac{z}{L}\right) \left[\left(\frac{\mathrm{d}u_x}{\mathrm{d}z}\right)^2 + \left(\frac{\mathrm{d}u_y}{\mathrm{d}z}\right)^2 \right] \mathrm{d}z, \\ V_P &= -\frac{P}{2} \int_0^L \left[\left(\frac{\mathrm{d}u_x}{\mathrm{d}z}\right)^2 + \left(\frac{\mathrm{d}u_y}{\mathrm{d}z}\right)^2 \right] \mathrm{d}z. \end{aligned} \tag{24}$$

Let $\Pi = U + V_q + V_P$ represent the total potential energy of the beam. The principle of minimum potential energy requires that

$$\delta \Pi = \delta(U + V_q + V_P) = 0. \tag{25}$$

Besides, the boundary conditions are

$$u_x|_{z=0} = u_y\big|_{z=0} = \phi_x|_{z=0} = \phi_y\big|_{z=0} = 0. \tag{26}$$

The finite element method is employed to solve the critical length of the pre-twisted beam. Discretize the beam into n_E equal-length elements along its longitudinal direction, with each element containing n_N nodes. Then the four generalized displacements can be represented by

$$\begin{aligned} u_x &= \sum_{i=1}^{n_\mathrm{N}} N_i(\xi) u_{1i}, \qquad u_y = \sum_{i=1}^{n_\mathrm{N}} N_i(\xi) u_{2i}, \\ \phi_x &= \sum_{i=1}^{n_\mathrm{N}} N_i(\xi) \phi_{1i}, \qquad \phi_y = \sum_{i=1}^{n_\mathrm{N}} N_i(\xi) \phi_{2i}, \end{aligned} \tag{27}$$

where u_{1i}, u_{2i}, ϕ_{1i}, and ϕ_{2i} are the generalized displacements at the i-th node, and the subscripts 1 and 2 labeling the x and y directions, respectively. $N_i(\xi)$ is the i-th shape function of the element and ξ is the local coordinate. Let z_t denote the z coordinate at the midpoint of the element t. The local coordinate ξ, varying in the range $[-1, 1]$, is expressed as

$$\xi = \frac{2}{l_\mathrm{E}}(z - z_t) = \frac{2z}{l_\mathrm{E}} - 2t + 1, \quad t = 1, 2, \cdots, n_\mathrm{E}, \tag{28}$$

where l_E is the length of the element. From Eq. (28), the derivative of the shape function with respect to z is

$$\frac{\mathrm{d}N_i(\xi)}{\mathrm{d}z} = \frac{\mathrm{d}N_i(\xi)}{\mathrm{d}\xi} \frac{\mathrm{d}\xi}{\mathrm{d}z} = \frac{2}{l_\mathrm{E}} \frac{\mathrm{d}N_i(\xi)}{\mathrm{d}\xi}. \tag{29}$$

Thus, the total potential energy Π in Eq. (25) is written as

$$\Pi = \sum_{t=1}^{n_\mathrm{E}} \Pi_t, \tag{30}$$

where Π_t is the potential energy of element t. Substituting Eqs. (27) and (30) into Eq. (25) results in

$$\begin{aligned} &\frac{\partial \Pi_t}{\partial u_{1i}} = \frac{\partial \Pi_t}{\partial u_{2i}} = \frac{\partial \Pi_t}{\partial \phi_{1i}} = \frac{\partial \Pi_t}{\partial \phi_{2i}} = 0, \\ &\quad t = 1, 2, \cdots, n_\mathrm{E}; \quad i = 1, 2, \cdots, n_\mathrm{N}. \end{aligned} \tag{31}$$

For element t, $4n_\mathrm{N}$ linear algebraic equations are then obtained as

$$\boldsymbol{K}^{(t)} \boldsymbol{d}^{(t)} = \boldsymbol{0}, \tag{32}$$

where $\boldsymbol{K}^{(t)}$ is the $4n_\mathrm{N} \times 4n_\mathrm{N}$ element stiffness matrix. Its nonzero components can be derived from Eqs. (28), (29), and (31) and are given in Appendix B. The $4n_\mathrm{N} \times 1$ node displacement column matrix $\boldsymbol{d}^{(t)}$ of element t is defined by

$$\begin{aligned} \boldsymbol{d}^{(t)} = [&u_{11}, u_{21}, \phi_{11}, \phi_{21}, \cdots, u_{1i}, u_{2i}, \phi_{1i}, \phi_{2i}, \cdots, \\ &u_{1n_\mathrm{N}}, u_{2n_\mathrm{N}}, \phi_{1n_\mathrm{N}}, \phi_{2n_\mathrm{N}}]^\mathrm{T}. \end{aligned} \tag{33}$$

Assembling the element matrices into the global matrix yields

$$\boldsymbol{K} \cdot \boldsymbol{d} = \boldsymbol{0}, \tag{34}$$

where $\boldsymbol{K}$ and $\boldsymbol{d}$ are the global stiffness matrix and node displacement column matrix, respectively. To impose the boundary conditions in Eq. (26), we remove the first four rows and columns of $\boldsymbol{K}$ and the first four rows of $\boldsymbol{d}$ and denote the reduced matrices as $\boldsymbol{K}_\mathrm{r}$ and $\boldsymbol{d}_\mathrm{r}$, respectively. Then Eq. (34) becomes

$$\boldsymbol{K}_\mathrm{r} \cdot \boldsymbol{d}_\mathrm{r} = \boldsymbol{0}. \tag{35}$$

It has an untrivial solution of $\boldsymbol{d}_\mathrm{r}$ only when the coefficient matrix $\boldsymbol{K}_\mathrm{r}$ is singular, i.e., $\det(\boldsymbol{K}_\mathrm{r}) = 0$. From this condition, the critical length of buckling of the pre-twisted beam can be obtained and denoted as L_cr.

It is emphasized that the above method allows us to easily examine the effects of twist angle, cross-sectional aspect ratio, and loading conditions on the buckling behavior of pre-twisted beams, as shown in the next section.

5 Results and discussions

5.1 Effect of chirality on bending deformation

For a pre-twisted cantilever beam under transverse bending, normalize its coupled deflections u_x and u_y by

$$\overline{u}_x = \frac{u_x}{L}, \quad \overline{u}_y = \frac{u_y}{L}. \tag{36}$$

Besides, let U_x and U_y denote the deflections in the x and y directions at the free end, respectively. Normalize them and the total deflection $U_{\text{total}} = \sqrt{U_x^2 + U_y^2}$ as

$$\bar{U}_x = \frac{U_x}{U_y^{(0)}}, \quad \bar{U}_y = \frac{U_y}{U_y^{(0)}}, \quad \bar{U}_{\text{total}} = \frac{U_{\text{total}}}{U_y^{(0)}}, \tag{37}$$

where $U_y^{(0)}$ denotes the value of U_y when $\theta = 0°$.

For example, we take the following parameters of the beam: length $L = 1\,\text{m}$, width $b = 0.01\,\text{m}$, thickness $h = 0.001\,\text{m}$ (cross-sectional aspect ratio $\mu = 10$), Young's modulus $E = 1\,\text{GPa}$, Poisson's ratio $\nu = 0.3$, and force intensity $\overline{f}_x = 0\,\text{N/m}^2$ and $\overline{f}_y = 0.1\,\text{N/m}^2$. The Fourier series in Eq. (19) is expanded to the first 20 terms. For different twisting angles $\theta = 0°$, 180°, 360°, and 720°, the normalized deflections $\overline{u}_x$ and $\overline{u}_y$ of the twisted beam are plotted in Fig. 3. The solid lines are calculated from our theoretical model, and the dots are obtained from finite element simulations. They have a good agreement, demonstrating the high accuracy of the analytical solution. At the free end, the deflection in the x direction is much smaller than that in the y direction. The deflection U_y of a pre-twisted beam (see the curves of $\theta = 180°$, 360°, and 720°) are distinctly smaller than that of a straight beam with $\theta = 0°$. Therefore, twisting a beam into a chiral morphology can greatly improve its resistance ability to bending.

Besides, let the thickness h change continuously from 0.01 to 0.001 m, corresponding to the change of the cross-sectional aspect ratio μ from 1 to 10. The variations of the normalized free-end deflections $\bar{U}_x$ and $\bar{U}_y$ with respect to μ are plotted in Fig. 4. For pre-twisted beams subjected to the distributed force in the y direction, both the normalized deflections $\bar{U}_x$ and $\bar{U}_y$ decrease with increasing θ, and the latter decreases more rapidly. When the beam has a square cross section (i.e., $\mu = 1$), the normalized deflections $\bar{U}_x = 0$ and $\bar{U}_y = 1$ will not vary with the twist angle θ.

Figure 5 shows that the improving effect of pre-twisting on the bending resistance of a beam becomes more and more substantial as θ increases from 180° to 720°. For example, the free-end deflection $\bar{U}_{\text{total}}$ of a pre-twisting beam with $\mu = 10$ and $\theta = 720°$ is lower about 64.9% than that of the corresponding flat beam. By setting $f_2 = 0$ and keeping the

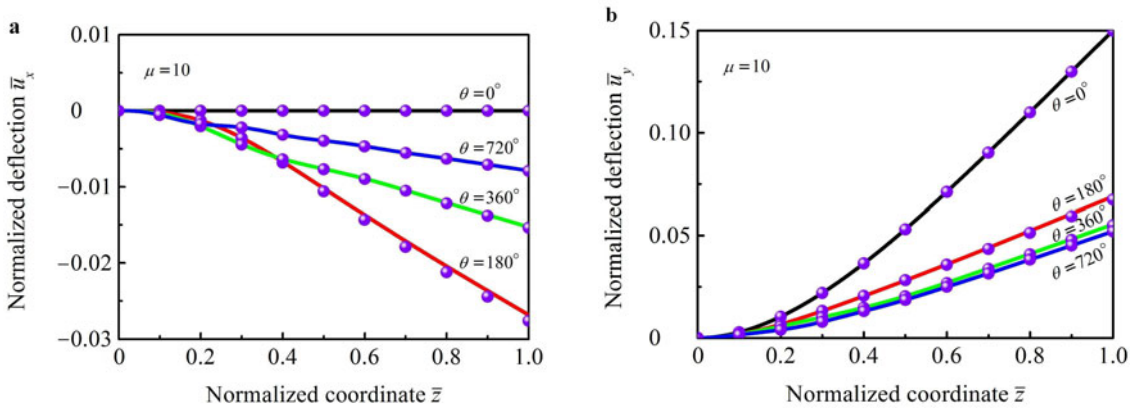

Fig. 3 Variations of the normalized deflections **a** $\overline{u}_x$ and **b** $\overline{u}_y$ of the beam with respect to the normalized coordinate $\overline{z}$, where the dots are the results from finite element simulations

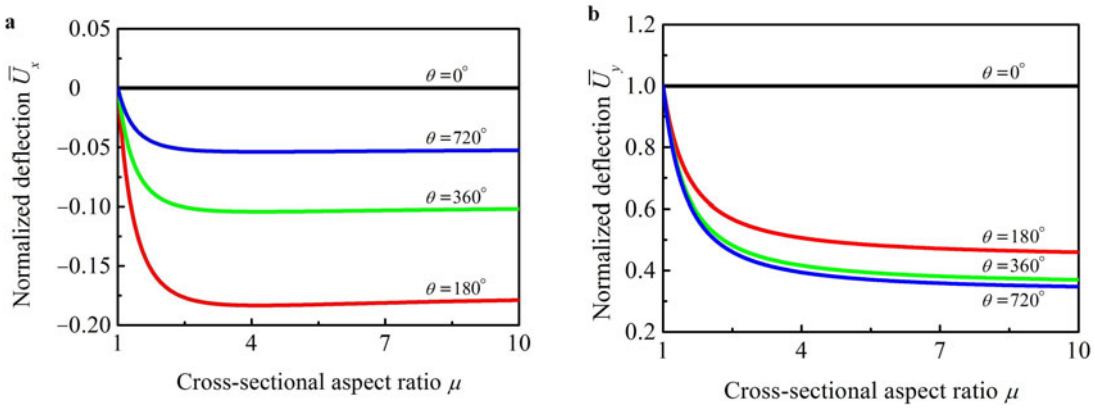

Fig. 4 Normalized deflections **a** $\bar{U}_x$ and **b** $\bar{U}_y$ at the free end as functions of the cross-sectional aspect ratio μ

other parameters unchanged, we further investigate the degenerated case that the pre-twisted beam is subjected to a uniformly distributed transvers force. The variations of the normalized free-end deflections $\bar{U}_{\text{total}}$ with regard to μ are complementally plotted in Fig. 5 with dashed lines. It is clear that for a specified μ, the normalized free-end deflection $\bar{U}_{\text{total}}$ induced by the periodically distributed force is much smaller than that induced by the uniformly distributed force. This indicates that both the smaller upstream area and the higher bending stiffness can be achieved by pre-twisting the beam.

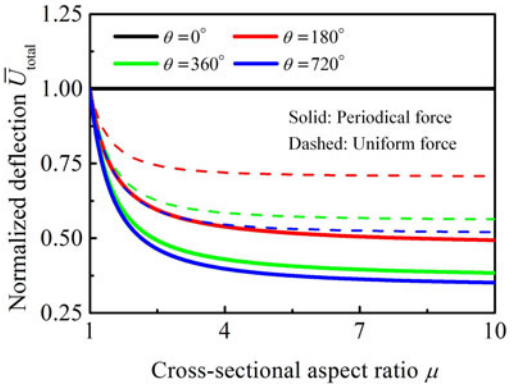

Fig. 5 Variations of the normalized deflections $\bar{U}_{\text{total}}$ of the beam with respect to the cross-sectional aspect ratio μ

5.2 Effect of chirality on axial buckling

In the buckling analysis of a slender beam subjected to the self-weight q and the concentrated compressive force P, introduce the dimensionless load ratio

$$\chi = \frac{P}{qL_{\text{ref}}}, \tag{38}$$

where L_{ref} is a reference length. Let L_0 and L_{cr} denote the critical buckling length for a straight and untwisted beam with $\theta = 0^\circ$ and a twisted beam, respectively. The dimensionless parameter

$$\eta = \frac{L_{\text{cr}}}{L_0} - 1 \tag{39}$$

is used to quantify the effect of twisting chirality on the critical length of buckling.

In the examples, we take the following representative values of geometric and material parameters: reference length $L_{\text{ref}} = 1\,\text{m}$, width $b = 0.01\,\text{m}$, thickness $h = 0.002\,\text{m}$ (cross-sectional aspect ratio $\mu = 5$), Young's modulus $E = 1\,\text{GPa}$, Poisson's ratio $\nu = 0.3$, mass density $\rho = 1 \times 10^3\,\text{kg/m}^3$, and gravitational acceleration $g = 10\,\text{N/kg}$. Three typical loading conditions with the load ratio $\chi = 0$, 1, and ∞ are compared, which correspond to (1) $P = 0$, $q > 0$; (2) $P = q > 0$; and (3) $P > 0$, $q = 0$, respectively.

The enhancing effect of twisting chiral morphology on the buckling length is shown in Fig. 6 in terms of the parameter η as a function of the twist angle θ. The results in the special case $\chi = 0$ coincide well with that of Nixdorff [30], who neglected the shear deformation effect. For untwisted beams (i.e., $\theta = 0^\circ$), the present result reduces to the classical Euler buckling solution based on the Timoshenko beam model [31]. It is seen from Fig. 6 that for twisted beams, η is always positive and increases with increasing twist angle θ. For example, in the case of $\theta = 720^\circ$ and $\chi = \infty$, the critical length L_{cr} increases about 33.5% due to the effect of twisting chirality. For a specified θ, the larger the load ratio χ, the higher the critical length L_{cr}. When $\theta = 720^\circ$, for instance, the value of η increases about 61.6% as χ changes from 0 to 1. Therefore, the enhancing effect of twisting chirality is more significant for a beam subjected to a concentrated force than that under a distributed force. Furthermore, it is noticed that the $\eta - \theta$ curves, especial when the concentrated force P is relatively large (e.g., $\chi = 1$ and $\chi = \infty$), show some slight wavy variations. This is reasonable and can be understood as follows. For the beam with a larger cross-sectional aspect ratio μ, the increase in the buckling length with increasing twist angle θ is non-uniform but has small fluctuations with a period of 180°.

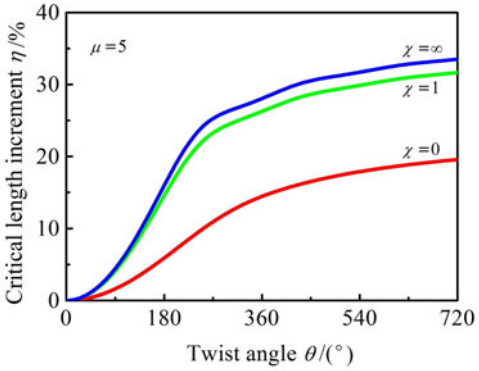

Fig. 6 Variations of the increment η of the beam as a function of the twist angle θ, where $\mu = 5$

In addition, we investigate the effect of cross-sectional aspect ratio μ on the buckling behavior of pre-twisted beams. For the fixed width $b = 0.01\,\text{m}$, we vary the thickness h from 0.01 to 0.001 m, corresponding to the increase of μ from 1 to 10. For three typical loading modes, the corresponding variations of the normalized critical length increment η with respect to μ are shown in Fig. 7. It is seen that η increases first rapidly and approaches a constant. Pre-twisting has no effect on the axial buckling resistance when the beam has a square cross section (i.e., $\mu = 1$). For a beam with larger μ, one can achieve a more significant enhancement in the critical buckling length by twisting it into a chiral morphology. For example, when $\mu = 10$, $\theta = 360^\circ$, and $\chi = \infty$, the critical buckling length L_{cr} of the twisted beam is about 29.4% larger than the corresponding straight and untwisted beam.

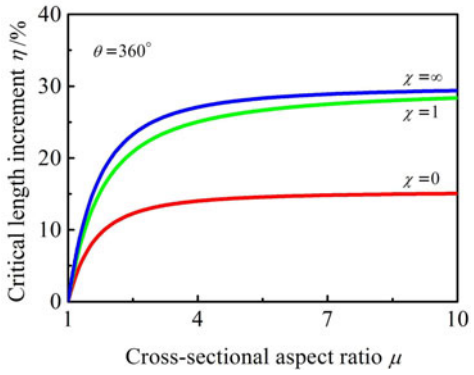

Fig. 7 Variations of the increment η of the beam with respect to the cross-sectional aspect ratio μ

6 Conclusions

This paper discusses the effect of twisting chiral morphology on the mechanical properties of beams, in particular, their transverse bending and axial buckling. An analytical solution has been derived for the deflections of a pre-twisted beam under periodically distributed transverse force. The critical buckling condition has also been obtained for a pre-twisted beam subjected to both self-weight and axial force. The results show that twisting a beam can significantly improve its resistance ability to both bending and Euler buckling. By this mechanism, such aquatic macrophytes as *Sagittaria trifolia* can grow higher, with efficient material utilization and superior ability against deformation and buckling. This also inspires us to design and optimize engineering devices (e.g., sensors and actuators) and structures with enhanced performance.

Appendix A: Parameters of Eq. (17)

The expressions of C_{1x}, C_{2x}, C_{1y}, and C_{2y} in Eq. (17) are given as

$$\begin{aligned}
C_{1x} &= \left[\frac{3}{2}-(\theta-\alpha)^2\right]\sin(2\alpha)+2(\theta-\alpha)\cos(2\alpha)\\
&\quad -2\theta+(2\theta^2-1)\alpha,\\
C_{2x} &= 2[10+2\cos(2\alpha)-9\cos(\theta-\alpha)\\
&\quad -9(\theta-\alpha)\sin\theta\cos\alpha]\sin\alpha\\
&\quad +18\alpha\left(\cos\theta+\theta\sin\theta-\frac{4}{3}\right),\\
C_{1y} &= 48\beta\theta^2\alpha(2\theta-\alpha)+2\alpha^2(1+\mu^2)(6\theta^2-4\theta\alpha+\alpha^2)\\
&\quad +3(1-\mu^2)\{[2(\theta-\alpha)^2-3]\cos(2\alpha)\\
&\quad +4(\theta-\alpha)\sin(2\alpha)+3-2\theta^2-4\theta\alpha\},\\
C_{2y} &= 288[(1+\beta\theta^2)(\cos\alpha-1)+\beta\theta^2\alpha\sin\theta]\\
&\quad +24\alpha^2(1+\mu^2)(3\cot\theta+3\theta-\alpha)\sin\theta\\
&\quad +4(1-\mu^2)\{56-54\cos\alpha-2\cos3\alpha\\
&\quad +9[\sin(2\alpha)-\alpha\cos(2\alpha)-\alpha\\
&\quad -2(\cot\theta+\theta)\sin^2\alpha]\sin\theta\}.
\end{aligned} \tag{A1}$$

Appendix B: Parameters of Eq. (32)

The non-zero components of $\boldsymbol{K}^{(t)}$ in Eq. (32) include

$$\begin{aligned}
K^{(t)}_{4(i-1)+1,4(j-1)+1} &= K^{(t)}_{4(i-1)+2,4(j-1)+2}\\
&= \frac{2\kappa GA}{EI_X l_{\mathrm{E}}}\int_{-1}^{1}\frac{\mathrm{d}N_i}{\mathrm{d}\xi}\frac{\mathrm{d}N_j}{\mathrm{d}\xi}\mathrm{d}\xi\\
&\quad -\frac{2(qn_{\mathrm{E}}l_{\mathrm{E}}+P)}{EI_X l_{\mathrm{E}}}\int_{-1}^{1}\frac{\mathrm{d}N_i}{\mathrm{d}\xi}\frac{\mathrm{d}N_j}{\mathrm{d}\xi}\mathrm{d}\xi\\
&\quad +\frac{2q}{EI_X}\int_{-1}^{1}\frac{z}{l_{\mathrm{E}}}\frac{\mathrm{d}N_i}{\mathrm{d}\xi}\frac{\mathrm{d}N_j}{\mathrm{d}\xi}\mathrm{d}\xi,\\
K^{(t)}_{4(i-1)+1,4(j-1)+4} &= K^{(t)}_{4(i-1)+2,4(j-1)+3}\\
&= -\frac{\kappa GA}{EI_X}\int_{-1}^{1}\frac{\mathrm{d}N_i}{\mathrm{d}\xi}N_j\mathrm{d}\xi,\\
K^{(t)}_{4(i-1)+3,4(j-1)+2} &= K^{(t)}_{4(i-1)+4,4(j-1)+1}\\
&= -\frac{2\kappa GA}{EI_X}\int_{-1}^{1}N_i\frac{\mathrm{d}N_j}{\mathrm{d}\xi}\mathrm{d}\xi,\\
K^{(t)}_{4(i-1)+3,4(j-1)+4} &= K^{(t)}_{4(i-1)+4,4(j-1)+3}\\
&= \frac{2(\mu^2-1)}{l_{\mathrm{E}}}\int_{-1}^{1}\sin\left(\frac{2\theta z}{n_{\mathrm{E}}l_{\mathrm{E}}}\right)\frac{\mathrm{d}N_i}{\mathrm{d}\xi}\frac{\mathrm{d}N_j}{\mathrm{d}\xi}\mathrm{d}\xi,\\
K^{(t)}_{4(i-1)+3,4(j-1)+3} &= \frac{\kappa GAl_{\mathrm{E}}}{EI_X}\int_{-1}^{1}N_iN_j\mathrm{d}\xi\\
&\quad +\frac{4}{l_{\mathrm{E}}}\int_{-1}^{1}\left[1+(\mu^2-1)\sin^2\left(\frac{\theta z}{n_{\mathrm{E}}l_{\mathrm{E}}}\right)\right]\frac{\mathrm{d}N_i}{\mathrm{d}\xi}\frac{\mathrm{d}N_j}{\mathrm{d}\xi}\mathrm{d}\xi,\\
K^{(t)}_{4(i-1)+4,4(j-1)+4} &= \frac{\kappa GAl_{\mathrm{E}}}{EI_X}\int_{-1}^{1}N_iN_j\mathrm{d}\xi\\
&\quad +\frac{4}{l_{\mathrm{E}}}\int_{-1}^{1}\left[1+(\mu^2-1)\cos^2\left(\frac{\theta z}{n_{\mathrm{E}}l_{\mathrm{E}}}\right)\right]\frac{\mathrm{d}N_i}{\mathrm{d}\xi}\frac{\mathrm{d}N_j}{\mathrm{d}\xi}\mathrm{d}\xi,
\end{aligned} \tag{A2}$$

$t=1,2,\cdots,n_{\mathrm{E}};\quad i,j=1,2,\cdots,n_{\mathrm{N}}.$

References

1 Oda, R., Huc I., Schmutz, M., et al.: Tuning bilayer twist using chiral counterions. Nature **399**, 566–569 (1999)

2 Ye, H.M., Wang, J.S., Tang, S., et al.: Surface stress effects on the bending direction and twisting chirality of lamellar crystals of chiral polymer. Macromole. **43**, 5762–5770 (2010)

3 Garcia-Ruiz, J.M., Melero-García, E., Hyde, S.T.: Morphogenesis of self-assembled nanocrystalline materials of barium carbonate and silica. Science **323**, 362–365 (2009)

4 Lotz, B., Gonthier-Vassal, A., Brack, A., et al.: Twisted single crystals of Bombyx mori silk fibroin and related model polypeptides with β structure: A correlation with the twist of the β sheets in globular proteins. J. Mol. Biol. **156**, 345–357 (1982)

5 Ji, X.Y., Zhao, M.Q., Wei, F., et al.: Spontaneous formation of double helical structure due to interfacial adhesion. Appl. Phys. Lett. **100**, 263104 (2012)

6 Paniagua, R., Royuela, M., Garcia-Anchuelo, R.M., et al.: Ultrastructure of invertebrate muscle cell types. Histol. Histopath. **11**, 181–201 (1996)

7 Wang, X., Sturegård, E., Rupar, R., et al.: Infection of BALB/c A mice by spiral and coccoid forms of Helicobacter pylori. J. Med. Microbiol. **46**, 657–663 (1997)

8 Wang, J.S., Wang, G., Feng, X.Q., et al.: Hierarchical chirality transfer in the growth of Towel Gourd tendrils. Sci. Rep. **3**, 3102 (2013)

9 Schulgasser, K., Witztum, A.: Spiralling upward. J. Theor. Biol. **230**, 275–280 (2004)

10 Schulgasser, K., Witztum, A.: The hierarchy of chirality. J. Theor. Biol. **230**, 281–288 (2004)

11 Chen, X., Yang, S., Motojima, S., et al.: Morphology and microstructure of twisting nano-ribbons prepared using sputter-coated Fe-base alloy catalysts on glass substrates. Mater. Lett. **59**, 854–858 (2005)

12 The *Paphiopedilum dianthum* picture is from the website of http://upload.wikimedia.org/wikipedia/commons/e/eb/Paphio-pedilum_dianthum_Orchi_15.eps.

13 Carnegie, W.: Vibrations of pre-twisted cantilever blading. Proc. Inst. Mech. Eng. **173**, 343–374 (1959)

14 Carnegie, W.: Vibrations of pre-twisted cantilever blading allowing for rotary inertia and shear deflection. J. Mech. Eng. Sci. **6**, 105–109 (1964)

15 Lin, S.C., Hsiao, K.M.: Vibration analysis of a rotating Timoshenko beam. J. Sound Vibr. **240**, 303–322 (2001)

16 Zhu, T.L.: The vibrations of pre-twisted rotating Timoshenko beams by the Rayleigh-Ritz method. Comput. Mech. **47**, 395–408 (2011)

17 Wang, J.S., Ye, H.M., Qin, Q.H., et al.: Anisotropic surface effects on the formation of chiral morphologies of nanomaterials. Proc. R. Soc. London Ser. A-Math. Phys. Eng. Sci. **468**, 609–633 (2012)

18 Carnegie, W.: Static bending of pre-twisted cantilever blading. Proc. Inst. Mech. Eng. **171**, 873–894 (1957)

19 Subrahmanyam, K.B., Kulkarni, S.V., Rao, J.S.: Static bending of pretwisted cantilever blading. In: Proceeding of the Indian Society of Theoretical and Applied Mechanics Twenty-Fourth Congress, 37–64 (1980)

20 Abid, S., Taktak, M., Dammak, F., et al.: An accurate two-node finite element for the pre-twisted beam modelling. J. Mech. Eng. **59**, 135–150 (2008)

21 Chen, W.R.: Bending behavior of twisted Timoshenko beams under distributed transverse loads. Hwa Kang J. Eng. Chin. Univ. **26**, 19–26 (2010)

22 Chen, W.R.: Parametric studies on bending of twisted Timoshenko beams under complex loadings. J. Mech. **28**, N1–N6 (2012)

23 Ziegler, H.: Die Knickung des verwundenen Stabes. Schweiz. Bauz. **66**, 463–465 (1948)

24 Ziegler, H.: Stabilitätsprobleme bei geraden Stäben und Wellen. ZAMP **2**, 265–289 (1951)

25 Lüscher, E.: Bemerkungen zur Knickung des verwundenen, einseitig eingespannten Stabes. Schweiz. Bauz. **71**, 172–173 (1953)

26 Leipholz, H.: Knickung verwundener Stäbe unter Druck einer konservativen, kontinuierlich und gleichmäßig verteilten Belastung. Arch. Appl. Mech. **29**, 262–279 (1960)

27 Nixdorff, K.: Zur Knickung verwundener Stäbe bei zusammengesetzter Belastung. Arch. Appl. Mech. **37**, 92–98 (1968)

28 Tabarrok, B., Yuexi, X., Steinman, D., et al.: On buckling of pretwisted columns. Int. J. Solids Struct. **26**, 59–72 (1990)

29 Cowper, G.R.: The shear coefficient in Timoshenko's beam theory. J. Appl. Mech. **33**, 335–340 (1966)

30 Nixdorff, K.: Neuere Ergebnisse zur Knickung verwundener Stäbe. Ing. Arch. **36**, 126–134 (1967)

31 Timoshenko, S.P., Gere, J.M.: Theory of Elastic Stability 2nd Edition. McGraw-Hill, New York (1961)